TISSUE ENGINEERING: Part A
Volume 23, Numbers 11 and 12, 2017

DOI: 10.1089/ten.tea.2016.0457

termis
Tissue Engineering
& Regenerative Medicine
International Society

ORIGINAL ARTICLE

Cell and Growth Factor-Loaded Keratin Hydrogels for Treatment of Volumetric Muscle Loss in a Mouse Model

H.B. Baker, PhD,[1,2,*] J.A. Passipieri, PhD,[2,3,*] Mevan Siriwardane, PhD,[2]
Mary D. Ellenburg, BS,[4] Manasi Vadhavkar, MS,[2] Christopher R. Bergman, BS,[2]
Justin M. Saul, PhD,[5] Seth Tomblyn, PhD,[4] Luke Burnett, PhD,[4] and George J. Christ, PhD[2,3,6]

Wounds to the head, neck, and extremities have been estimated to account for ~84% of reported combat injuries to military personnel. Volumetric muscle loss (VML), defined as skeletal muscle injuries in which tissue loss results in permanent functional impairment, is common among these injuries. The present standard of care entails the use of muscle flap transfers, which suffer from the need for additional surgery when using autografts or the risk of rejection when cadaveric grafts are used. Tissue engineering (TE) strategies for skeletal muscle repair have been investigated as a means to overcome current therapeutic limitations. In that regard, human hair-derived keratin (KN) biomaterials have been found to possess several favorable properties for use in TE applications and, as such, are a viable candidate for use in skeletal muscle repair. Herein, KN hydrogels with and without the addition of skeletal muscle progenitor cells (MPCs) and/or insulin-like growth factor 1 (IGF-1) and/or basic fibroblast growth factor (bFGF) were implanted in an established murine model of surgically induced VML injury to the latissimus dorsi (LD) muscle. Control treatments included surgery with no repair (NR) as well as implantation of bladder acellular matrix (BAM). *In vitro* muscle contraction force was evaluated at two months postsurgery through electrical stimulation of the explanted LD in an organ bath. Functional data indicated that implantation of KN+bFGF+IGF-1 ($n=8$) enabled a greater recovery of contractile force than KN+bFGF ($n=8$)***, KN+MPC ($n=8$)**, KN+MPC+bFGF+IGF-1 ($n=8$)**, BAM ($n=8$)*, KN+IGF-1 ($n=8$)*, KN+MPCs+bFGF ($n=9$)*, or NR ($n=9$)**, (*$p<0.05$, **$p<0.01$, ***$p<0.001$). Consistent with the physiological findings, histological evaluation of retrieved tissue revealed much more extensive new muscle tissue formation in groups with greater functional recovery (e.g., KN+IGF-1+bFGF) when compared with observations in tissue from groups with lower functional recovery (i.e., BAM and NR). Taken together, these findings further indicate the general utility of KN biomaterials in TE and, moreover, specifically highlight their potential application in the treatment of VML injuries.

Keywords: volumetric muscle loss, IGF, FGF, keratin hydrogel, myogenesis

Introduction

Skeletal muscle injuries and disorders that result in permanent loss of function have been defined as volumetric muscle loss (VML) injuries by Grogan *et al.*[1] Such injuries are common among active military personnel wherein head, neck, and extremity wounds constitute an estimated 84% of all combat injuries to military personnel.[2–4] In addition to trauma to wounded warriors and civilians (e.g., car accidents, gunshot wounds), VML or VML-like injuries can also arise as a result of excision of cancerous tissue, congenital birth defects such as cleft lip and cleft palate, and as a result of acquired diseases such as Bell's palsy.[5–8]

Presently, the gold standard of treatment for VML is an autologous or cadaveric muscle graft. While these interventions have become increasingly successful with advances in

[1]Fischell Department of Bioengineering, University of Maryland, College Park, Maryland.
[2]Wake Forest Institute for Regenerative Medicine, Wake Forest University, Winston-Salem, North Carolina.
[3]Department of Biomedical Engineering, University of Virginia, Charlottesville, Virginia.
[4]KeraNetics, LLC, Winston-Salem, North Carolina.
[5]Department of Chemical, Paper and Biomedical Engineering, Miami University, Oxford, Ohio.
[6]Department of Orthopaedics, University of Virginia, Charlottesville, Virginia.
*These authors contributed equally to this work.

microsurgery, flap transfer procedures still suffer from donor–host compatibility issues in the case of cadaveric tissue and from donor site morbidity when using autologous tissues.[9–11] Current efforts in tissue engineering (TE) research seek to develop therapeutic approaches that overcome these limitations and provide functional improvements that are capable of better meeting the needs of the wide variety of VML presentations.

In this regard, researchers have investigated several biomaterial scaffolds, including synthetic and biologically derived materials, for use in skeletal muscle indications.[12–17] Biologically derived materials are of particular interest in TE applications due to their availability and favorable structural and chemical characteristics.[18–20] Investigators have applied a variety of biologic materials alone or in concert with cells, drugs, or growth factors in several different animal models of muscle injury.[21,22] Among these approaches, extracellular matrix (ECM)-derived materials have shown promise for use in TE applications, and a number of devices consisting of ECM materials have been FDA approved for several indications, including soft tissue repair, rotator cuff reinforcement, and superficial wound healing.[18]

Previous work in our group has focused on the use of a decellularized, porcine-derived bladder acellular matrix (BAM) scaffold coupled with cells and physiologic preconditioning *in vitro* before implantation in rodent models of VML injury. This implantable technology, referred to as a tissue-engineered muscle repair (TEMR) construct, produced a significant improvement in functional recovery from VML injuries to both the latissimus dorsi (LD) and tibialis anterior muscles.[23–25] In further building a platform of technologies capable of treating a wider variety of VML injuries, our group has begun to explore other biologic scaffold materials, including the keratin hydrogels that are the subject of this study.

Keratin biomaterials have a host of properties favorable for regenerative medicine applications and pertinent to skeletal muscle repair. For example, isolated keratin proteins have been shown to improve cell attachment[26,27] and reductively isolated keratins (kerateines) have been found to promote platelet adhesion and coagulation.[28] In addition, keratin hydrogels are capable of achieving sustained release of drugs and growth factors.[29–31] Cell differentiation from monocytes to pro-regeneration type II macrophages has also been shown to occur in the presence of keratin biomaterials.[32] Not surprisingly, keratin biomaterials have shown positive results in several regenerative medicine applications, including burn healing,[33,34] bone regeneration,[30,35] and nerve regeneration.[36–38]

Keratin proteins have shown promise in applications of TE, generally using alpha and gamma trichocytic keratins extracted from human hair. The alpha fraction makes up the majority of hair fibers, with the beta fraction present in the cortex of the fibers, while the globular gamma fraction provides the supporting matrix around filaments.[20] The keratins can be solubilized through disruption of the disulfide bonds to open the cortex and denature the fibers into constitutive proteins through either an oxidative or reductive process.[39,40]

Oxidative extraction yields keratins with altered cysteine residues that can no longer cross-link with other keratins and are referred to as keratose. Reductive isolation results in keratin referred to as kerateine in which the cysteine group disulfide bonds are broken, but the cysteine residues are unaltered and able to reform disulfide bonds. As a result of these properties, keratose has a faster degradation rate than kerateine[39,40] and the two can be combined to achieve a desired degradation rate.[41]

In the current study, several properties of keratin hydrogels were utilized in developing and employing a construct to promote muscle repair. Keratin hydrogels made up of kerateine and keratose were combined in a manner to achieve degradation within 2 months while simultaneously permitting sustained release of growth factors over this time frame. In addition, keratin hydrogels served as a delivery vehicle for autologous skeletal muscle progenitor cells (MPCs) to the site of injury.

Insulin-like growth factor-1 (IGF-1) and basic fibroblast growth factor (bFGF) were chosen for investigation based upon their known effects on the skeletal muscle cell population. More specifically, IGF-1 has been demonstrated to promote differentiation of satellite cells and fusion of myoblasts, while studies using bFGF indicated that it promotes satellite cell activation and proliferation; these effects have been thoroughly discussed and summarized elsewhere.[42–46]

The overriding hypothesis of this study was that keratin hydrogels would promote functional improvement of skeletal muscle in the VML injury setting by encouraging a more favorable microenvironment for tissue repair and regeneration. It was further hypothesized that the addition of MPCs as well as growth factors (IGF-1 and bFGF) would complement and enhance the regenerative capacity of keratin alone. To investigate these hypotheses, keratin hydrogels, with or without the addition of a cellular component, growth factors, or a combination of both, were examined in an established murine model of VML injury for their ability to enable restoration of function and native tissue morphology.

Materials and Methods

Keratin extraction

Keratins were extracted using a patented process in a quality system regulation/good manufacturing process, QSR/GMP, facility at KeraNetics, LLC (Winston Salem, NC). Briefly, a cold solution of 0.5 M thioglycolic acid in sodium hydroxide (reductive extraction for kerateine) or a 2% peracetic acid (PAA) solution (oxidative extraction for keratose) was added to end cut human hair.

For reductive extraction, the reducing solution was added to hair in a mixing tank for 12 h at 37°C, followed by two washes in 100 mM Tris base (Sigma) and water. The solution was then centrifuged, filtered, dialyzed against a 100 kDa molecular weight cutoff cellulose membrane, and neutralized to pH 7.4. For oxidative extraction with PAA, the hair was handled in a similar manner. Following acid extraction and Tris base/water washes, the extract was purified by centrifugation and dialyzed in water against a 50 kDa nominal low-molecular-weight cutoff membrane. Both the oxidized and reduced solutions were lyophilized, ground, and sterilized by gamma irradiation.

BAM preparation

BAM scaffolds were prepared as previously described.[25] Briefly, porcine-derived bladder was washed and trimmed to

obtain the lamina propria, which was placed in 0.05% trypsin (Hyclone, Logan, UT) for 1 h at 37°C. The bladder was then transferred to Dulbecco's modified Eagle's medium (DMEM); the solution was supplemented with 10% fetal bovine serum (FBS) and 1% antibiotic–antimycotic, AA (Hyclone), and kept overnight at 4°C.

The preparation was then washed in a solution containing 1% Triton-X (Sigma) and 0.1% ammonium hydroxide (Fisher Scientific, Pittsburgh, PA) in deionized water for 4 days at 4°C. Finally, the bladder was then washed in deionized water for 3 days at 4°C. The decellularized scaffold was further dissected to obtain a scaffold of 0.2–0.4 mm thickness. The scaffolds were then cut and draped onto custom-made silicone molds with a 4.5 cm^2 working area.

MPC culture

Mouse MPCs were isolated from the tibialis anterior and soleus muscles of 4–8-week-old male C57/Bl6 mice purchased from Charles River Laboratories. Muscles were sterilized in iodine and washed with phosphate-buffered saline (PBS) before transfer to a 0.2% w/v collagenase (Worthington Biochemical, Lakewood, NJ) low-glucose DMEM (Hyclone) solution where they were finely minced and then allowed to further digest at 37°C for 2 h. The cell slurry was plated on Matrigel (BD Biosciences, San Jose, CA)-coated tissue culture plastic in myogenic media consisting of high-glucose DMEM supplemented with 20% fetal bovine FBS, 10% horse serum (HS), 1% chick embryo extract, and 1% AA (Hyclone). Three days after plating, the media were changed to seeding media consisting of low-glucose DMEM supplemented with 15% FBS and 1% AA (Hyclone). At 70–80% confluence, cells were passaged.

KSO (keratose):KTN (kerateine) optimization and cell capacity

We have previously investigated the release of growth factors from variable ratios of KSO to KTN through ELISA analysis of solution surrounding growth factor-loaded hydrogels.[41,47] The gels were prepared with selected ratios of KSO to KTN, in which varied concentrations (w/v) of keratin powder to sterile PBS were also examined. The results indicated that a 70:30 blend of 15% KSO and 7% KTN resulted in the sustained release of both IGF-1 and bFGF over the course of one month, results which were further examined in a mouse *in vivo* study.[47]

Based on rheology data reported by Tomblyn *et al.*,[47] the elastic modulus of a hydrogel that allows incorporation of cells and may still be extruded through a surgical syringe is $\sim$100 Pa. The maximum number of cells that could be incorporated into the optimized blend and still yield a hydrogel flowable in nature and capable of being extruded through a surgical syringe was 1.7×10^6 MPCs/mL in the KSO fraction. It may be assumed that addition of this concentration of cells resulted in a hydrogel that did not have an elastic modulus significantly greater than 100 Pa. As such, it is worth noting that the viscosity of the hydrogel limited the concentration of cells used in this study.

Hydrogel preparation

For the growth factor-containing groups, IGF-1 and/or bFGF (Peprotech, Rocky Hill, NJ) were diluted in sterile water to yield a final concentration of 100 μg/mL of each growth factor. Growth factor solutions were added to KTN powders to make a 7% w/v hydrogel. KSO was added to either PBS or a serum-free medium cell suspension of $\sim1.65\times10^6$/mL passage 2 mouse MPCs to form a 15% w/v hydrogel. The KTN and KOS hydrogels were then combined at a 70:30 KSO:KTN ratio by passing the gels between coupled syringes.

Treatment groups

Treatment groups and group sizes are listed in Table 1 and are as follows: no repair (NR) $n=9$, treatment with BAM $n=8$, keratin (KN) $n=6$, KN+IGF-1 (KN+I) $n=8$, KN+bFGF (KN+b) $n=8$, KN+I+b $n=8$, KN+MPCs (KN+M) $n=8$, KN+M+I $n=8$, KN+M+b $n=9$, and KN+M+I+b $n=8$. IGF-1 and bFGF were loaded at a concentration of 100 μg/mL hydrogel, and cells were seeded at a density of $\sim1.65\times10^6$/mL hydrogel.

Animal care

This study was conducted in compliance with the Animal Welfare Act, the Implementing Animal Welfare Regulations,

Table 1. Design of Experimental Groups Submitted to Latissimus Dorsi Volumetric Muscle Loss Injury Model: List of Groups, Components, and Number of Animals (*n*) is Described

Treatment group (abbreviation)	*Number of animals* (n)	*Components*			
		Keratin	*MPCs*	*IGF-1*	*bFGF*
NR	9				
BAM	8				
Keratin (KN)	6	+			
Keratin+IGF-1 (KN+I)	8	+		+	
Keratin+bFGF (KN+b)	8	+			+
Keratin+IGF1+bFGF (KN+I+b)	8	+		+	+
Keratin+MPC (KN+M)	8	+	+		
Keratin+MPC+IGF-1 (KN+M+I)	8	+	+	+	
Keratin+MPC+bFGF (KN+M+ b)	9	+	+		+
Keratin+MPC+IGF-1+bFGF (KN+M+I+b)	8	+	+	+	

KN, keratin; I: IGF-1, insulin-like growth factor 1; b: bFGF, basic fibroblast growth factor; M: MPC, muscle progenitor cell; BAM, bladder acellular matrix; NR, no repair.

and in accordance with the principles of the Guide for the Care and Use of Laboratory Animals. The Wake Forest University Health Sciences School of Medicine Animal Care and Use Committee approved all animal procedures. A total of 80 female C57/BL6 mice (Charles River Laboratories) weighing 19.1 ± 0.3 g at 8–10 weeks old were individually housed in a vivarium accredited by the American Association for the Accreditation of Laboratory Animal Care and provided with food and water *ad libitum*.

Mouse LD VML model and hydrogel implant

The VML model was created by resecting $\sim 50\%$ of the area of the LD muscle, which is $\sim 16 \pm 3$ mg, as was done in previous studies.[23,24] After defect creation, animals were randomly assigned to one of the following treatment groups: NR, BAM, keratin alone, and keratin with a combination of cells, IGF-1, and bFGF (groups listed in Table 1, surgery shown in Fig. 1). For the BAM treatment, scaffolds were folded and secured with 6–0 vicryl (Ethicon, Somerville, NJ) at the proximal and distal ends of the defect. For the NR and keratin groups, after creation of the defect, the fascia and mammary fat pad were closed with 6–0 vicryl. For treatment with keratin hydrogels, 0.1–0.2 mL of the hydrogel was injected into the fascial pocket over the injury site. In all groups, the skin was then sutured with 5–0 prolene (Ethicon) and animals were allowed to recover.

At 2 months postimplant, animals were sacrificed, and the experimental and contralateral LD muscles were explanted for functional and histological analyses.

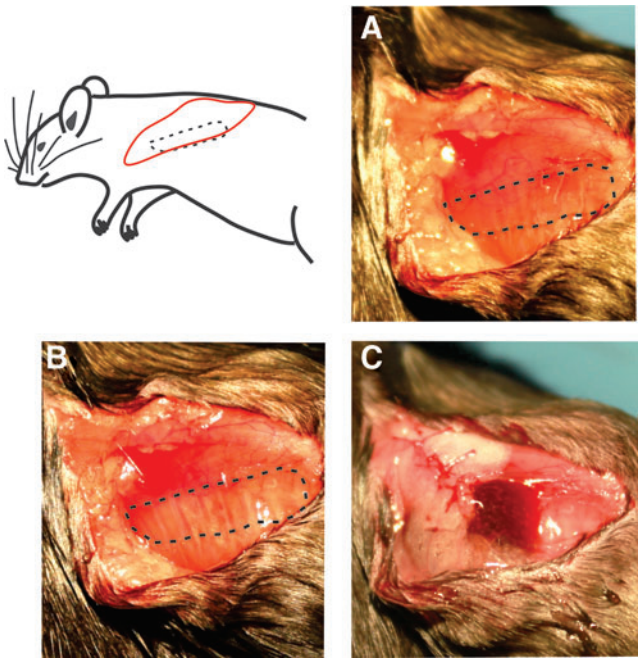

FIG. 1. Surgical flow of volumetric muscle loss injury and keratin implant. Muscle is isolated in **(A)** with the proposed defect region *outlined*; defect is created and *outlined* in **(B)**. Fascia is partially closed and keratin hydrogel is injected into the fascial pocket **(C)**. Fascia and skin are then closed and the animal is allowed to recover. Color images available online at www.liebertpub.com/tea

Muscle function analysis

While under anesthesia, the entire LD muscle of each mouse was isolated from the thoracolumbar fascia to the humeral tendon and the tendon and facial ends were tied with 5–0 silk suture (Ethicon) and transferred to ice-cold Krebs–Ringer buffer solution (Sigma; composition: pH 7.4; concentration in mM: 121.0 NaCl, 5.0 KCl, 0.5 $MgCl_2$, 1.8 $CaCl_2$, 24.0 $NaHCO_3$, 0.4NaH2PO_4, and 5.5 glucose). Muscles were transferred to individual chambers of a DMT 750 tissue organ bath system (DMT, Ann Arbor, MI) filled with Krebs–Ringer buffer at 35°C bubbled with 95% O_2 and 5% CO_2. The muscles were positioned between custom-made platinum electrodes with the proximal tendon attached to a force transducer and the distal tendon to a fixed support. Direct muscle electrical stimulation (0.2 ms pulse at 30 V) was applied across the LD muscle using a Grass S88 stimulator (Grass, Warwick, RI).

Real-time display and recording of all force measurements were performed on a PC with Power Lab/8sp (AD Instruments, Colorado Springs, CO). Once the LD muscles were mounted in the organ bath, the muscles were allowed to equilibrate for 5 min before determining optimal physiological muscle length (L_o) through a series of twitch contractions. Force as a function of stimulation frequency (1–250 Hz) was measured at 37°C during isometric contractions (750 ms trains of 0.2 ms pulses), with 2 min between contractions. The maximal force of contraction, P_o, was normalized to an approximate physiological cross-sectional area (PCSA), which was calculated using the following equation, where muscle density is 1.06 g/cm^3:

Equation 1. Physiological cross-sectional area (PCSA) calculation.

$$PCSA = (wet\ weight\ (g)/ \left[muscle\ density\ \left(g/cm^3\right) \times muscle\ length, L_o\ (cm)\right]$$

Additionally, the force–frequency curves were fit to the following dose–response equation:

$$f(x) = min - (max - \min)/[1 + (x/EC_{50})^{-n}],$$

Equation 2. Dose–response formula.

where x is the stimulation frequency in Hz, *min* is the lowest observed force generated, equivalent to the twitch force or P_t, max is the largest observed force or P_o, EC_{50} is the stimulation frequency, which yields half the amplitude of the maximum observed force (P_o-P_t), and n is the slope of the linear portion of the force–frequency curve. Additionally, submaximal tetanic contraction at 80 Hz (P_{80Hz}) is included in Table 2. Of note, tissues that were inadvertently damaged during retrieval or testing were not included in the contraction measurement data.

Histology, immunohistochemistry, and imaging

Muscles from all experimental groups were photographed before fixation in 4% paraformaldehyde overnight at 4°C and embedding in paraffin wax. Tissue sections were taken within the plane of the LD muscle and imaged as shown in Figure 2. Hematoxylin and eosin and Masson's trichrome stains were conducted by standard techniques to determine

Table 2. Summary of Latissimus Dorsi Muscle Physical and Functional Measurement Data

Treatment group	*Uninjured*	*NR*	*BAM*	*KN*	*KN+I*	*KN+b*	*KN+I+b*	*KN+M*	*KN+M+I*	*KN+M+b*	*KN+M+I+b*	*ANOVA p-value*
Sample size (*n*)	41	9	8	6	8	8	8	8	8	9	8	
Muscle characteristics												
Wet weight (mg)	75.7 ± 2.0	66.1 ± 9.9	134.8 ± 19.2[a,b,d,e,g-k]	71.2 ± 12.0	82.6 ± 10.9	107.4 ± 19.7[a,b,g,i]	72.0 ± 2.6	84.7 ± 16.7	60.7 ± 7.8	91.3 ± 10.6	97.6 ± 23.9[i]	0.0007
L_o (mm)	33.3 ± 0.8[b,c,f,i,k]	27.9 ± 1.5	32.6 ± 1.1[b,d]	27.8 ± 0.7	30.0 ± 0.7	28.4 ± 1.5	30.1 ± 1.3	30.5 ± 1.1	28.3 ± 2.1	30.3 ± 1.7	28.9 ± 1.6	0.0048
PCSA (mm^2)	2.2 ± 0.1	2.2 ± 0.3	3.8 ± 0.5[a,b,d,e,g-i]	2.4 ± 0.4	2.6 ± 0.3	3.7 ± 0.8[a,b,d,g,i]	2.3 ± 0.1	2.6 ± 0.5	2.0 ± 0.2	2.9 ± 0.4	3.2 ± 0.7[a,i]	0.0028
Isometric force parameters												
P_t meas. (mN)	30.6 ± 0.9[l]	13.6 ± 1.6	12.1 ± 1.4	12.6 ± 2.7	13.9 ± 2.3	10.9 ± 1.8	17.4 ± 2.5[f,h,k]	11.4 ± 1.4	15.4 ± 1.4	12.5 ± 1.8	11.4 ± 2.2	<0.0001
P_{80Hz} meas. (mN)	188.4 ± 4.6[l]	67.9 ± 10.7	78.5 ± 9.9	82.7 ± 16.5	74.3 ± 14.5	71.0 ± 15.7	99.6 ± 13.8	76.1 ± 11.9	94.6 ± 11.9	73.6 ± 13.4	70.0 ± 16.0	<0.0001
P_o meas. (mN)	290.1 ± 4.0	123.2 ± 12.5	148.0 ± 15.7	161.6 ± 19.4	148.7 ± 29.1	115.9 ± 20.1	198.8 ± 21.4[b,c,e,f,h,j,k]	127.3 ± 16.5	157.0 ± 20.9	141.6 ± 21.0	125.3 ± 21.2	<0.0001
Specific P_o (N/cm^2)	13.7 ± 0.4[l]	6.3 ± 1.1	4.3 ± 0.7	7.3 ± 0.9	6.6 ± 1.6	4.3 ± 1.1	9.1 ± 1.4[c,f]	6.1 ± 1.3	8.0 ± 1.1[c,f]	6.1 ± 1.5	6.1 ± 2.2	<0.0001
EC_{50} (Hz)	69.2 ± 0.2[l]	81.0 ± 2.1	82.0 ± 1.8	85.8 ± 3.5[f,h,i]	88.1 ± 4.1[b,f,h,i]	76.0 ± 3.0	91.0 ± 2.8[b,c,f,h,i]	75.5 ± 3.0	75.5 ± 2.2	86.3 ± 2.2[f,h,i]	85.3 ± 3.8[f,h,i]	<0.0001
n coefficient	3.4 ± 0.03	3.5 ± 0.3	3.5 ± 0.2	2.9 ± 0.3	3.3 ± 0.4	3.8 ± 0.5	3.1 ± 0.3	2.7 ± 0.3	3.5 ± 0.3	3.4 ± 0.3	3.2 ± 0.4	0.2647

Values are mean ± standard error of the mean. Muscle mass was measured after completion of functional testing. L_o is the optimal muscle length associated with peak twitch response (P_t). PCSA was determined using the measured L_o and wet weight using Equation (1). Peak twitch (P_t), contraction force at 80 Hz (P_{80}), and maximal isometric contraction force (P_o) were measured by soliciting contractions through direct electric stimuli (0.2 ms, 30 V) in the organ bath setup. Measured P_o was normalized to PCSA to determine specific force (Specific P_o). The stimulation frequency, which yielded 50% of the absolute maximum amplitude (EC_{50}), and the slope of the linear portion of the force–frequency curves shown in Figure 3 (*n* coefficient) were determined by fitting the curves to function described by Equation (2). Superscript denotations indicate statistically different group means ($p < 0.05$) from [a]uninjured, [b]NR,[c]BAM,[d]KN,[e]KN+IGF-1, [f]KN+ bFGF, [g]KN+IGF-1+bFGF, [h]KN+MPC, [i]KN+MPC+IGF-1, [j]KN+MPC+bFGF, [k]KN+MPC+IGF-1+bFGF, and [l]all other groups.

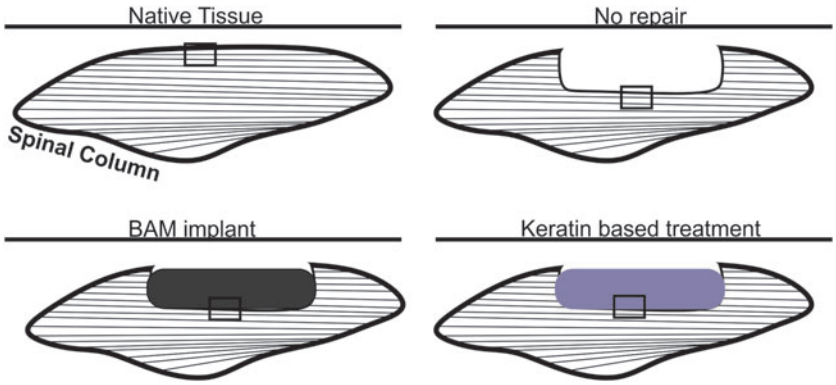

FIG. 2. Depiction of location of tissue sections for use in histological analyses. Tissues were sectioned longitudinally in the same plane as the length of the LD muscles at 5 μm thickness. Images were taken at the regions indicated with *rectangles* in the figure to include the interface between uninjured and treated tissue with native tissue in the lower portion of each image. LD, latissimus dorsi. Color images available online at www.liebertpub.com/tea

the basic morphology of cells in and around the implant and to observe any inflammatory response. Implants retrieved from three animals in each treatment group were studied.

Immunohistochemical staining was performed by using antibody to detect myosin (MF-20, 1:10) acquired from Developmental Studies Hybridoma Bank, Iowa City, IA. Biotinylated anti-mouse IgG (MKB-2225, 1:250, Vector Laboratories, Inc.) secondary antibody was used to detect primary antibodies. The sections were next treated with avidin–biotin complex reagent (PK-7100, Vector Laboratories, Inc.) and then visualized using a NovaRED substrate kit (SK-4800, Vector Laboratories, Inc.). Finally, the sections were counterstained using Gill's hematoxylin (GHS280, Sigma-Aldrich). Tissue sections without primary antibody were used as negative controls. Images were captured and digitized (DM4000B Leica Upright Microscope) at varying magnifications.

Statistical analysis

Numeric data are presented as mean ± SEM. Functional data were statistically analyzed by one-way ANOVA. When significance was found ($p < 0.05$), a *post hoc* multiple comparison test was used to compare group means ($p < 0.05$) using a Fisher least significant difference (LSD) significance test. Statistical analysis was conducted using GraphPad Prism 6.0 for Windows (La Jolla, California).

Results

Creation of VML injury and in vitro *functional assessment*

None of the animals died as a result of the surgical procedure and no postimplantation mortality was recorded. The weights of the LD muscles excised from the animals in each treatment group were not statistically different ($p = 0.135$), reflecting the creation of comparable VML injuries (NR: 16.2 ± 0.6 mg; BAM: 14.9 ± 0.7 mg; KN: 14.5 ± 0.7 mg; KN+I: 16.5 ± 1.3 mg; KN+b: 16.8 ± 0.5 mg; KN+I+b: 15.6. ± 1.3 mg; KN+M: 14.3 ± 0.8 mg; KN+ M+I: 18.4 ± 1.3 mg; KN+M+b: 16.3 ± 0.7 mg; KN+M+I+b: 15.4 ± 0.9 mg).

In vitro force measurement was conducted 2 months postimplantation on both experimental and contralateral control muscles harvested from all 10 treatment groups outlined in Table 1. Mean values for all parameters of interest derived from retrieved LD muscles of all animals are listed in Table 2, and statistical comparison of mean values for P_o and specific P_o is graphically displayed in Figure 3. The VML injury created in this study resulted in a 58% ± 4.3% reduction in maximum isometric contraction force (P_o), a 56% ± 5.1% reduction in peak twitch force (P_t), and a 64% ± 5.7% reduction in measured submaximal tetanic contraction at 80 Hz (P_{80Hz}) in the NR group relative to uninjured control muscles (Table 2).

Among all of the treatment groups, implantation of KN+I+b was associated with the greatest mean value for P_o, P_t, and P_{80Hz} and, furthermore, had the highest specific P_o (Table 2). Statistical analysis revealed that the mean P_o values measured for KN+I+b treatment group were significantly greater than the corresponding values in all other treatment groups except for KN and KN+M+I (Fig. 3). The mean measured P_t values for the KN+I+b treatment group were also significantly greater than KN+b, KN+M, and KN+M+I+b, and furthermore, the mean specific P_o values for the KN+I+b treatment groups were significantly greater than the corresponding BAM and KN + b mean values. In addition, the KN+M+I treatment group also had mean specific P_o values that were significantly higher than those observed in the BAM and KN + b treatment groups (Fig. 3).

Consistent with a previous report,[23] analysis of curve fits to force–frequency data documented significant increases in EC_{50} values for all treatments relative to control values, although with no detectable differences in curve slope (n) among any of the groups (Table 2). The mean EC_{50} value for the KN+I+b treatment group had the largest shift relative to uninjured values and was significantly different than the mean EC_{50} values for NR, BAM, KN+b, KN+M, and KN+M+I treatment groups. Also of note, at the time of tissue retrieval, the mass of LD muscles from the BAM treatment group was significantly greater than any treatment group except KN + b and was also significantly greater than control LD mass equating to 178% ± 25% of control values.

The LD muscles from the KN + b treatment group were also significantly heavier than that of several treatment groups (Table 2), with a mean value of 142% ± 26% relative to the corresponding mean value for uninjured control tissues. Significant differences in optimal muscle length (L_o) were also detected among the treatment groups. More specifically, among the treatment groups, only the LD muscles retrieved from the BAM treatment group had a significantly greater mean L_o value than that of the NR group, although it is worth noting that several keratin-treated groups, including

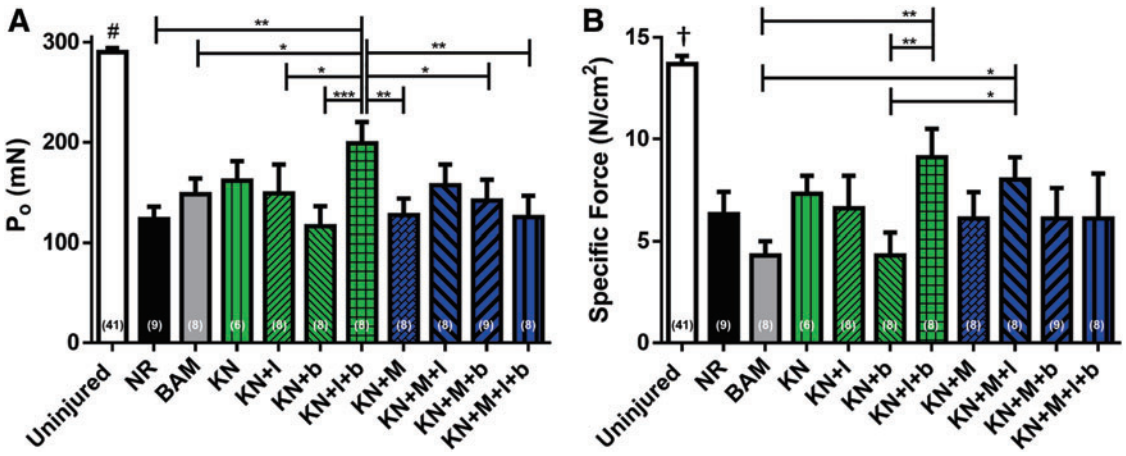

FIG. 3. Muscle function analysis at 2 months postsurgery. Maximum isometric contraction force (P_0) as a result of electrical field stimulation (1–250 Hz, 0.2 ms, 30 V) **(A)**; normalized to PCSA **(B)**. For both measurements, uninjured contralateral control muscles $n=41$, NR $n=9$, BAM $n=8$, KN $n=6$, KN+I $n=8$, KN+b $n=8$, KN+I+b $n=8$, KN+M $n=8$, KN+M+I $n=8$, KN+M+b $n=9$, and KN+M+I+b $n=8$. Acellular hydrogel treatment groups are colored *green*, cellularized hydrogel treatment groups are *colored blue*. Significant differences are denoted as follows: $*p<0.05$, $**p<0.01$, $***p<0.001$, † different from all other groups $p<0.001$, and #different from all other groups $p<0.0001$. NR, no repair; BAM, bladder acellular matrix. Color images available online at www.liebertpub.com/tea

the KN+I+b animals, had mean L_o values, which were not significantly different from those observed in uninjured control muscles.

To better frame the nature of the functional recovery observed in this study with prior work from our group in a similar, although immune-incompetent, murine LD VML injury model,[23,24] we have graphed the complete frequency–response curves for the KN+I+b group versus that of native LD, as well as NR and BAM-implanted animals (Fig. 4). As shown, 2 months after implantation of this KN hydrogel formulation, we observed a statistically significant increase in contraction throughout the majority of the frequency–response curve when compared with the NR and/or BAM treatment groups (which were not different from each other). This clearly illustrates the magnitude of functional recovery that can be achieved with KN hydrogels, which is ~70% of the maximal response observed in native LD muscle.

Whole tissue morphology

Upon completion of functional studies and physical measurements, retrieved tissues from all animals and treatment groups were photographed. Representative examples from each treatment group are shown in Figure 5. Among treatment groups, variable degrees of volume recovery were observed. All KN treatment groups as well as BAM-implanted animals had obvious signs of vascularization in the implant area at the macroscopic level.

Histology and immunochemistry

Retrieved tissues from three animals in each treatment group were sectioned and stained with hematoxylin and eosin, Masson's trichrome, or myosin heavy chain. An illustration of how the VML defect was created and treated with the keratin implant is shown in Figure 1, and a schematic illustration of the regions of interest studied through histology is provided in Figure 2. As indicated, specific attention was paid to identify the interface between the implant (or injured area in the NR; indicated by dashed yellow line) and the native muscle tissue.

The rationale for this analytical approach is that in this VML injury model, all of the tissue is removed from a contiguous section of the LD muscle parallel to the

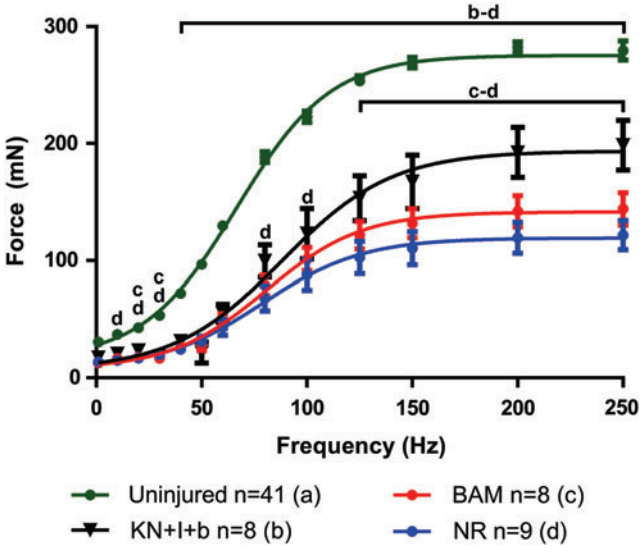

FIG. 4. Selected force–frequency curves with fitted dose–response curves. At 2 months postsurgery, contractions were elicited through electrical stimuli from 1 to 250 Hz as shown for uninjured, KN+I+b, BAM, and NR muscles. Dose–response data have been curve fit according to Equation (2). Curve fitting was used to determine EC_{50} and Hill Slope values shown in Table 2. *Letters above* group curves denote groups that were statistically different at a given data point; *brackets* indicate differences were observed for all points included in the span of the *bracket*; $p<0.05$; a: Uninjured; b: KN+I+b; c: BAM; d: NR. Color images available online at www.liebertpub.com/tea

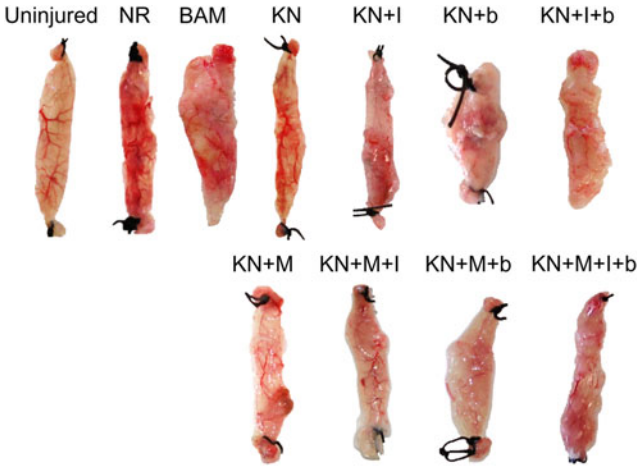

FIG. 5. Representative tissue gross morphology. Images shown were taken following functional assessment carried out at 2 months postsurgery. Representative samples from each group are shown. Color images available online at www.liebertpub.com/tea

remaining native tissue (Figs. 1 and 2). The keratin hydrogel (or BAM) is then injected (or sutured) into the pocket created by surgical excision of the muscle tissue, and the fascia is closed with sutures (Fig. 1C).

For the NR and BAM treatment groups, identification of the interface with the native tissue was quite straightforward because the NR animals had little or no new tissue in the excised region, while the BAM-treated animals had little or no new muscle tissue in the implanted region. Of note with respect to the keratin-implanted mice, for example, no new muscle tissue is expected beyond the borders of the remaining native tissue in the absence of *de novo* tissue regeneration as the hydrogel degrades during the 2-month course of study.

Depicted in Figure 6 are representative images obtained in tissue sections of the LD muscle retrieved at the 2-month time point from both control and selected experimental groups. Figure 6A–C shows the normal architecture of the mouse LD muscle in the same region as the section that was surgically removed to create the VML injury. Figure 6D–F shows the periphery of the remaining native LD muscle from an NR mouse. As illustrated, there was little or no evidence of new tissue formation observed in the NR mouse following surgical excision, although a minimal amount of adipose tissue and collagen deposition was noted at the edge of the native tissue adjacent to the defect region (Fig. 6E, F respectively).

In contrast, in BAM-treated muscles (Fig. 6G–I), a much greater volume of collagen was observed in the surgically created defect area well beyond the native tissue interface. Within the collagenous region (indicated with #), there are apparently dispersed mononuclear cells present with no obvious muscle tissue organization, although minimal evidence of *de novo* muscle tissue formation was occasionally detected contiguous with the edge of the native tissue (data not shown).

New tissue formation was much more notable among the keratin treatment groups and consisted of varying amounts of collagen, adipose tissue, mononuclear cells, and neomuscle

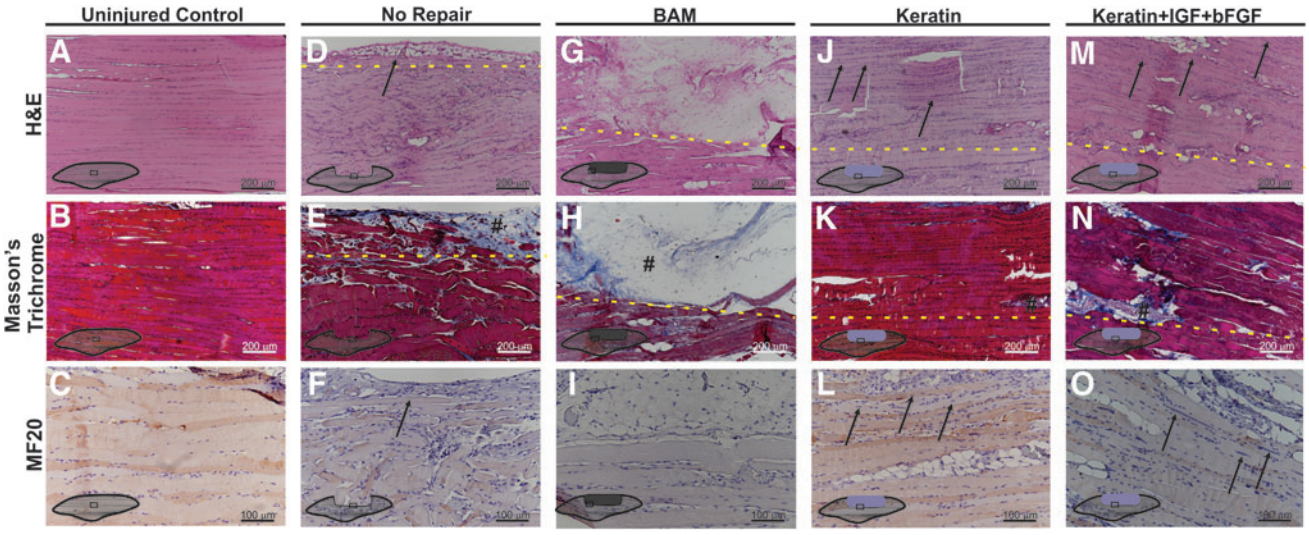

FIG. 6. Representative examples of mouse LD cell and tissue morphology and functional protein expression. **(A–C)** Uninjured control, **(D–F)** NR, **(G–I)** BAM, **(J–L)** KN, and **(M–O)** KN+I+b. Cell and tissue morphology was examined through hematoxylin and eosin staining **(A, D, G, J, M)** wherein nuclei are stained *blue-purple* and cytoplasm and cellular proteins are stained *pink*. Collagen deposition was examined through Masson's trichrome staining **(B, E, H, K, N)**, in which tissue stains *red*, collagen stains *blue*, and nuclei stain *black*. The presence of new muscle tissue formation within the defect and treatment site was evaluated by staining for myosin (MF-20) **(C, F, I, L, O)**; (#) denotes collagen deposition; new muscle formation is indicated with *black arrows*; and *yellow dashed lines* indicate the interface between native and remodeling tissue. It is important to note that even in the case of relatively robust new muscle tissue formation, the interface between the newly formed skeletal muscle and the native tissue was quite readily identified by the greater deposition of extracellular collagen and/or adipose tissue, as well as the presence of smaller muscle fibers, which frequently exhibited branching profiles and centrally located nuclei (Fig. 7). Color images available online at www.liebertpub.com/tea

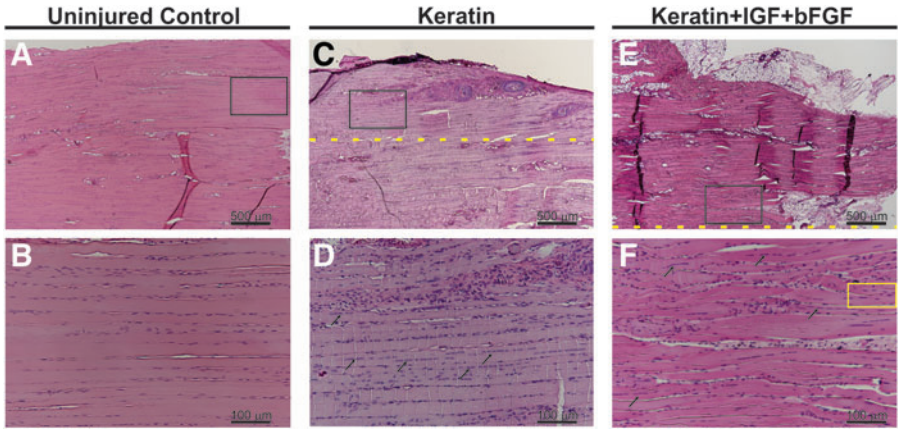

FIG. 7. Histological evidence of newly regenerated muscle fibers in keratin and keratin+IGF+bFGF-treated muscles. Hematoxylin and eosin stain of representative samples from the uninjured control groups **(A, B)**, KN-treated **(C, D)**, and KN+I+b-treated groups **(E, F)** highlighting the skeletal muscle morphology observed in native and newly formed (regenerating) muscle tissue postimplantation. As shown, **(B, D, F)** represent the higher magnification image of *black boxes* in **(A, C, E)**, respectively. *Arrows* denote examples of muscle fibers with centrally located nuclei in the KN implant region. The *yellow box encircles* a representative example of a branching fiber, although such fibers were identified throughout the implant region. *Yellow dashed lines* indicate the interface between native and regenerating/remodeling tissue. Color images available online at www.liebertpub.com/tea

tissue formation. Representative examples of KN-treated animals are also shown in Figure 6. Consistent with the functional studies (Figs. 3 and 4), KN-treated tissues showed a greater extent of *de novo* muscle tissue formation compared with BAM and NR groups.

It is important to note that even in the case of the relatively robust new muscle tissue formation observed in the KN-treated animals, the border between the remaining native tissue and newly formed muscle tissue was quite readily identified. This border showed more extracellular collagen and/or adipose tissue deposition among the detectable striated muscle fibers, as well as the presence of smaller fibers that frequently exhibited branching profiles and centrally located nuclei, both of which are hallmarks of muscle regeneration.[48] However, even well beyond the border of the defect site (dashed lines in Fig. 6), numerous muscle fibers (black arrows) traveling along the long axis of the native tissue are evident with thinner fibers observed at the outermost edge of the neotissue, although with less structural organization than observed in the remaining native muscle.

The main implication is that in the keratin-treated groups, most obviously for the KN+I+b treatment (Fig. 6M–O), the most robust average functional recovery (i.e., increased contraction) was observed in the presence of the greatest amount of *de novo* muscle tissue formation in the implanted area of the VML injury (Figs. 3 and 4).

Discussion

In previous studies, our group developed two distinct models of VML injury in rodents to examine the effectiveness of regenerative medicine/TE approaches to muscle repair. Specifically, we focused on evaluating a TEMR technology platform as a potential treatment for VML injury.[23–25] In this scenario, a BAM scaffold is loaded with MPCs and subjected to cyclic stretch preconditioning in a customized bioreactor before implantation. Implantation of TEMR is associated with recovery of ~70% of the native contractile response within 2–3 months postimplantation and with significant skeletal muscle regeneration. With these established rodent models in hand as a baseline for comparison, it is possible to evaluate additional technologies, such as keratin hydrogels, as potential therapeutics for VML injuries.

Development and evaluation of multiple potential technologies for treatment of VML injuries seem prudent in light of the complexity of these injuries and the resulting variation in functional and cosmetic deficits that can occur. In this regard, keratin is a viable candidate for VML repair due to its capacity to serve as an injectable cell and drug delivery vehicle.[26,28,31,32,35,37]

As alluded to above, there is now a significant extant literature documenting that the inclusion of a cellular component in TE strategies for VML repair provides improved functional outcomes when compared with implantation of decellularized matrices/biomaterials alone.[23–25,49–55] Our group has documented this in two distinct VML injury models, in both immune-competent rats[25] (tibialis anterior muscle) and nude mice[23,24] (LD muscle).

Others have reported similar findings with distinct decellularized extracellular matrices, highlighting the fact that modest functional improvements are clearly possible following ECM implantation alone, although they are generally associated with little, if any, evidence for robust *de novo* muscle regeneration.[56–58] Investigators have also shown that growth factors alone, or coupled with cell and scaffold-based therapies, can improve muscle recovery after injury *in vivo*.[52,59,60] Such observations, in conjunction with corresponding *in vitro* investigations, highlight the potentially important role of, for example, IGF-1 and bFGF, in skeletal muscle regeneration.[44–46] Taken together, this body of work provided the underlying rationale for the current investigation.

Functional studies *in vitro* indicated that the combination of keratin, IGF-1, and bFGF (KN+I+b) resulted in the

greatest overall recovery in EFS-induced contraction after injury at 2 months postimplantation (Figs. 3 and 4; Table 2). Interestingly, this treatment also yielded the greatest recovery of absolute and specific contractile force in the absence of a cellular component. In fact, overall, it seems clear from Figure 3 and Table 2 that the inclusion of cells in the keratin hydrogel provided little apparent additional functional benefit over the hydrogel alone or the hydrogel in combination with IGF-1 and/or bFGF. Similar results with KN+I+b were obtained in the companion article to this work, which used a rat tibialis anterior VML injury model.[61]

Our current observations beg the question as to why the inclusion of MPCs in the KN hydrogel provided little detectable functional improvement in the same VML injury model(s). Of note, our studies did use donor male cells implanted into female recipients. The rationale for this approach was to minimize the requirements for donor animals (given the larger muscle sizes in males) and to ensure comparison with our prior studies.[23–25] In this regard, there are reports of the potential importance of gender differences in muscle stem cells.[62–63] While we cannot unequivocally rule out a potential role for gender differences in muscle-derived stem cells in our current observations, our previously published observations have reported robust functional regeneration in the same animal models of VML injury using the same approach.

As such, the most likely reasons for the reported findings are twofold. First, our prior work included mechanical preconditioning (i.e., bioreactor-induced cyclic stretch) and culturing in differentiation medium before implantation to induce formation of myotubes.[23–25] In the current study, cells were combined with keratin immediately after culture expansion (i.e., no bioreactor preconditioning). Second, in our prior work, implanted scaffolds carried $\sim 6 \times 10^6$ MPCs (1×10^6 MPCs/cm^2 per side on a 1×3 cm construct) compared with $\sim 1.2–2.3 \times 10^5$ MPCs in the injected volume of hydrogel used in this study. This constitutes a 26–50-fold reduction in cell number in the current study. This low cell concentration is the maximum we could achieve given the viscosity requirement of the hydrogel that could be dispensed (and held in place) into the injury in a 200 μL hydrogel volume.

These practical constraints likely precluded critical cell–cell interactions that are possible in the monolayer of myoblasts and myotubes characteristic of the TEMR scaffold that was implanted in our prior studies.[23–25] In short, it would appear that the lower cell concentration coupled with the absence of mechanical preconditioning may have mitigated the beneficial functional effects typically attributed to cell-based therapies.[23–25,64] Although the present study did not containing mechanical preconditioning, it is important to recognize the role of matrix stiffness in directing cellular behavior, including differentiation for both stem cells[65–66] and muscle satellite cells.[67]

We have recently demonstrated[41] that the keratin hydrogel formulation used in this study has an elastic modulus of ~ 1.5 kPa. It has previously been shown that matrix stiffness in this range is suitable for satellite cell differentiation and therefore the keratin formulations used in these studies are not expected to impede cellular differentiation. However, it is important to note that previous studies have used polyethylene glycol (PEG) hydrogels that are synthetic in nature and lack cell binding motifs found in keratin. As such, optimization of the keratin stiffness is an avenue for future research.

To further frame the nature and extent of the functional recovery observed following implantation of KN hydrogels, we plotted the complete frequency response curves for the KN+I+b group versus that of native LD, as well as NR and BAM-implanted animals (Fig. 4). The rationale for emphasizing this subset of experiments is that the KN+I+b group displayed the greatest degree of functional recovery (as judged by the number of statistically significant differences in contractile force from all other treatment groups), and furthermore, the degree of functional recovery observed was comparable with that previously seen for the TEMR technology.[23,24]

As illustrated, at 2 months postimplantation, a statistically significant increase in contraction throughout the majority of the frequency–response curve was observed compared with the contractile responses observed for retrieved LD muscles from NR and/or BAM treatment groups. This observation clearly confirms and extends our prior work to document that $\sim 70\%$ recovery of the maximal response observed in native LD muscle is achievable following VML injury in this animal model using a distinct regenerative technology.

It is also important to highlight that in the companion article to this work,[61] implantation of KN+I+b in a rat TA VML injury model had exactly the same functional outcome (again, not significantly different from KN alone) among the same treatment groups in another immune-competent animal model. While the precise mechanism responsible for the KN+I+b treatment group in two distinct VML injury models, in two different species, is not precisely known, the implications of these findings are of obvious importance to improved functional muscle regeneration and will be further explored in future investigations.

Whole tissue images (Fig. 5) of retrieved implants indicated a wide range of tissue reconstitution among the various treatment groups. Histological evaluation also indicated the ability of keratin treatments to support favorable tissue remodeling and muscle regeneration. For example, KN+I+b tissues showed evidence of robust new muscle tissue formation (Fig. 6M–O), consisting of abundant *de novo* muscle fibers, which extended from the borders of the native tissue well into the region where muscle was surgically excised. This observation stands in stark contrast to results in the NR and BAM groups (Fig. 6D–F, G–I) where new muscle tissue formation was rarely observed and, even then, was visible only as a thin layer along the border of the injury nearest the native tissue.

Although we recognize that both IGF and bFGF are pleiotropic peptides with numerous potential effects on skeletal muscle regeneration,[42,46,52,59,60,68–70] the selected doses in the current investigation were based on previous results *in vitro* and in a subcutaneous rodent model[47] and clearly have a positive impact on the regenerative microenvironment in this VML injury model. Clearly, future investigations will be required to further delineate the mechanism(s) responsible for the current observations and to further optimize the use of growth factors for an even greater degree of functional recovery in the setting of VML injury.

Taken together, these observations have shown, for the first time, the important implications of a tunable KN hydrogel

biomaterial platform for improved therapeutics for VML injuries and VML-like conditions. Future work will be aimed at optimization of the KN formulation for growth factor delivery as well as for inclusion of a cellular component, each of which could provide further improvements in functional muscle regeneration. Additionally, further studies will be required to evaluate the durability of the functional regeneration beyond the 2-month time point studied herein.

Finally, these studies provide further credence for the results shown in the companion article to this work,[61] in that implantation of KN+I+b in a rat TA VML injury model had exactly the same functional outcome (again, indistinguishable from KN alone) among the same treatment groups as it does following implantation in a mouse model of VML injury. The major implication of these initial studies is that utilization of a tunable KN hydrogel biomaterial platform provides another promising strategy for functional muscle regeneration and repair in the setting of VML injury.

Acknowledgments

The authors would like to thank Ms. Catherine Okoukoni, Ms. Caroline Stewart, and Mr. Daniel Lovell for technical assistance during surgery and functional testing and for technical assistance with histological procedures. J.A.P. acknowledges support as a CNPq Postdoctoral Fellow (2013–2014).

Disclosure Statement

No competing financial interests exist.

References

1. Grogan, B.F., and Hsu, J.R.; Skeletal Trauma Research Consortium. Volumetric muscle loss. J Am Acad Orthop Surg **19**, S35, 2011.
2. Covey, D.C. Blast and fragment injuries of the musculoskeletal system. J Bone Joint Surg Am **84-A,** 1221, 2002.
3. Masini, B.D., Waterman, S.M., Wenke, J.C., Owens, B.D., Hsu, J.R., and Ficke, J.R. Resource utilization and disability outcome assessment of combat casualties from operation Iraqi Freedom and operation enduring freedom. J Orthop Trauma **23,** 261, 2009.
4. Owens, B.D., Kragh, J.F., Jr., Wenke, J.C., Macaitis, J., Wade, C.E., and Holcomb, J.B. Combat wounds in operation Iraqi freedom and operation enduring freedom. J Trauma **64,** 295–299, 2008.
5. Thiele, O.C., Seeberger, R., Engel, M., Freier, K., and Hoffmann, J. Development of the clinical use of distant flaps for head and neck reconstruction. J Craniomaxillofac Surg **42,** 79, 2014.
6. Muramatsu, K., Ihara, K., Doi, K., Yoshida, K., Iwanaga, R., Hashimoto, T., and Taguchi, T. Functional neurovascularized muscle transfer for oncological reconstruction of extremity sarcoma. Surg Oncol **21,** 263, 2012.
7. Fisher, D.M., and Sommerlad, B.C. Cleft lip, cleft palate, and velopharyngeal insufficiency. Plast Reconstr Surg **128,** 342E, 2011.
8. Baugh, R.F., Basura, G.J., Ishii, L.E., Schwartz, S.R., Drumheller, C.M., Burkholder, R., Deckard, N.A., Dawson, C., Driscoll, C., Gillespie, M.B., Gurgel, R.K., Halperin, J., Khalid, A.N., Kumar, K.A., Micco, A., Munsell, D., Rosenbaum, S., and Vaughan, W. Clinical Practice Guideline: bell's Palsy. Otolaryngol Head Neck Surg **149,** S1, 2013.
9. Bianchi, B., Copelli, C., Ferrari, S., Ferri, A., and Sesenna, E. Successful salvage surgery after treatment failures with cross graft and free muscle transplant in facial reanimation. J Craniomaxillofac Surg **40,** 185, 2012.
10. Lawson, R., and Levin, L.S. Principles of free tissue transfer in orthopaedic practice. J Am Acad Orthop Surg **15,** 290, 2007.
11. Can, A., Orgill, D.P., Ulrich, J.O.D., and Mureau, M.A.M. The myocutaneous trapezius flap revisited: a treatment algorithm for optimal surgical outcomes based on 43 flap reconstructions. J Plast Reconstr Aesthet Surg **67,** 1669, 2014.
12. Cezar, C.A., and Mooney, D.J. Biomaterial-based delivery for skeletal muscle repair. Adv Drug Deliv Rev **84,** 188, 2015.
13. Qazi, T.H., Mooney, D.J., Pumberger, M., Geissler, S., and Duda, G.N. Biomaterials based strategies for skeletal muscle tissue engineering: existing technologies and future trends. Biomaterials **53,** 502, 2015.
14. Juhas, M., and Bursac, N. Engineering skeletal muscle repair. Curr Opin Biotechnol **24,** 880, 2013.
15. Rossi, C.A., Pozzobon, M., and De Coppi, P. Advances in musculoskeletal tissue engineering moving towards therapy. Organogenesis **6,** 167, 2010.
16. Yan, W., George, S., Fotadar, U., Tyhovych, N., Kamer, A., Yost, M.J., Price, R.L., Haggart, C.R., Holmes, J.W., and Terracio, L. Tissue engineering of skeletal muscle. Tissue Eng **13,** 2781, 2007.
17. Wolf, M.T., Dearth, C.L., Sonnenberg, S.B., Loboa, E.G., and Badylak, S.F. Naturally derived and synthetic scaffolds for skeletal muscle reconstruction. Adv Drug Deliv Rev **84,** 208, 2015.
18. Brown, B.N., and Badylak, S.F. Extracellular matrix as an inductive scaffold for functional tissue reconstruction. Transl Res **163,** 268, 2014.
19. Altman, G.H., Diaz, F., Jakuba, C., Calabro, T., Horan, R.L., Chen, J.S., Lu, H., Richmond, J., and Kaplan, D.L. Silk-based biomaterials. Biomaterials **24,** 401, 2003.
20. Rouse, J.G., and Van Dyke, M.E. A review of Keratin-based biomaterials for biomedical applications. Materials **3,** 999, 2010.
21. Vigodarzere, G.C., and Mantero, S. Skeletal muscle tissue engineering: strategies for volumetric constructs. Front Physiol **5,** 13, 2014.
22. Turner, N.J., and Badylak, S.F. Regeneration of skeletal muscle. Cell Tissue Res **347,** 759–774, 2012.
23. Corona, B.T., Machingal, M.A., Criswell, T., Vadhavkar, M., Dannahower, A.C., Bergman, C., Zhao, W.X., and Christ, G.J. Further development of a tissue engineered muscle repair construct in vitro for enhanced functional recovery following implantation in vivo in a murine model of volumetric muscle loss injury. Tissue Eng Part A **18,** 1213, 2012.
24. Machingal, M.A., Corona, B.T., Walters, T.J., Kesireddy, V., Koval, C.N., Dannahower, A., Zhao, W.X., Yoo, J.J., and Christ, G.J. A tissue-engineered muscle repair construct for functional restoration of an irrecoverable muscle injury in a murine model. Tissue Eng Part A **17,** 2291, 2011.
25. Corona, B.T., Ward, C.L., Baker, H.B., Walters, T.J., and Christ, G.J. Implantation of in vitro tissue engineered muscle repair constructs and bladder acellular matrices partially restore in vivo skeletal muscle function in a rat model of volumetric muscle loss injury. Tissue Eng Part A **20,** 705, 2014.
26. Tachibana, A., Furuta, Y., Takeshima, H., Tanabe, T., and Yamauchi, K. Fabrication of wool keratin sponge scaffolds for long-term cell cultivation. J Biotechnol **93,** 165, 2002.

27. Verma, V., Verma, P., Ray, P., and Ray, A.R. Preparation of scaffolds from human hair proteins for tissue-engineering applications. Biomed Mater **3,** 12, 2008.
28. Burnett, L.R., Rahmany, M.B., Richter, J.R., Aboushwareb, T.A., Eberli, D., Ward, C.L., Orlando, G., Hantgan, R.R., and Van Dyke, M.E. Hemostatic properties and the role of cell receptor recognition in human hair keratin protein hydrogels. Biomaterials **34,** 2632, 2013.
29. Peyton, C.C., Keys, T., Tomblyn, S., Burmeister, D., Beumer, J.H., Holleran, J.L., Sirintrapun, J., Washburn, S., and Hodges, S.J. Halofuginone infused keratin hydrogel attenuates adhesions in a rodent cecal abrasion model. J Surg Res **178,** 545, 2012.
30. de Guzman, R.C., Saul, J.M., Ellenburg, M.D., Merrill, M.R., Coan, H.B., Smith, T.L., and Van Dyke, M.E. Bone regeneration with BMP-2 delivered from keratose scaffolds. Biomaterials **34,** 1644, 2013.
31. Saul, J.M., Ellenburg, M.D., de Guzman, R.C., and Van Dyke, M. Keratin hydrogels support the sustained release of bioactive ciprofloxacin. J Biomed Mater Res Part A **98A,** 544, 2011.
32. Fearing, B.V., and Van Dyke, M.E. In vitro response of macrophage polarization to a keratin biomaterial. Acta Biomater **10,** 3136, 2014.
33. Poranki, D.R., and Van Dyke, M.E. The effect of gamma keratose on cell viability in vitro after thermal stress and the regulation of cell death pathway-specific gene expression. Biomaterials **35,** 4646, 2014.
34. Poranki, D., Whitener, W., Howse, S., Mesen, T., Howse, E., Burnell, J., Greengauz-Roberts, O., Molnar, J., and Van Dyke, M. Evaluation of skin regeneration after burns in vivo and rescue of cells after thermal stress in vitro following treatment with a keratin biomaterial. J Biomater Appl **29,** 26, 2014.
35. Kowalczewski, C.J., Tombyln, S., Wasnick, D.C., Hughes, M.R., Ellenburg, M.D., Callahan, M.F., Smith, T.L., Van Dyke, M.E., Burnett, L.R., and Saul, J.M. Reduction of ectopic bone growth in critically-sized rat mandible defects by delivery of rhBMP-2 from kerateine biomaterials. Biomaterials **35,** 3220, 2014.
36. Sierpinski, P., Garrett, J., Ma, J., Apel, P., Klorig, D., Smith, T., Koman, L.A., Atala, A., and Van Dyke, M. The use of keratin biomaterials derived from human hair for the promotion of rapid regeneration of peripheral nerves. Biomaterials **29,** 118, 2008.
37. Pace, L.A., Plate, J.F., Mannava, S., Barnwell, J.C., Koman, L.A., Li, Z., Smith, T.L., and Van Dyke, M. A human hair keratin hydrogel scaffold enhances median nerve regeneration in nonhuman primates: an electrophysiological and histological study. Tissue Eng Part A **20,** 507, 2014.
38. Pace, L.A., Plate, J.F., Smith, T.L., and Van Dyke, M.E. The effect of human hair keratin hydrogel on early cellular response to sciatic nerve injury in a rat model. Biomaterials **34,** 5907, 2013.
39. Hill, P., Brantley, H., and Van Dyke, M. Some properties of keratin biomaterials: kerateines. Biomaterials **31,** 585, 2010.
40. de Guzman, R.C., Merrill, M.R., Richter, J.R., Hamzi, R.I., Greengauz-Roberts, O.K., and Van Dyke, M.E. Mechanical and biological properties of keratose biomaterials. Biomaterials **32,** 8205, 2011.
41. Ham, T.R., Lee, R.T., Han, S., Haque, S., Vodovotz, Y., Gu, J., Burnett, L.R., Tomblyn, S., and Saul, J.M. Tunable keratin hydrogels for controlled erosion and growth factor delivery. Biomacromolecules **17,** 225, 2016.
42. Charge, S.B.P., and Rudnicki, M.A. Cellular and molecular regulation of muscle regeneration. Physiol Rev **84,** 209, 2004.
43. Bischoff, R. Chemotaxis of skeletal muscle satellite cells. Dev Dyn **208,** 505, 1997.
44. Florini, J.R., Ewton, D.Z., and Coolican, S.A. Growth hormone and the insulin-like growth factor system in myogenesis. Endocr Rev **17,** 481, 1996.
45. Hayashi, S., Aso, H., Watanabe, K., Nara, H., Rose, M.T., Ohwada, S., and Yamaguchi, T. Sequence of IGF-I, IGF-II, and HGF expression in regenerating skeletal muscle. Histochem Cell Biol **122,** 427, 2004.
46. Allen, R.E., and Andboxhorn, L.K. Regulation of skeletal-muscle satellite cell-proliferation and differentiation by transforming growth factor-beta, insulin-like growth factor-I, and fibroblast growth-factor. J Cell Physiol **138,** 311, 1989.
47. Tomblyn, S., Kneller, E.L.P., Walker, S.J., Ellenburg, M.D., Kowalczewski, C.J., Van Dyke, M., Burnett, L., and Saul, J.M. Keratin hydrogel carrier system for simultaneous delivery of exogenous growth factors and muscle progenitor cells. J Biomed Mater Res B Appl Biomater **104,** 864, 2016.
48. Hawke, T.J., and Garry, D.J. Myogenic satellite cells: physiology to molecular biology. J Appl Physiol **91,** 534, 2001.
49. Corona, B.T., Wu, X., and Walters, T.J. Treatment of volumetric muscle loss injury with muscle-derived ECM and BMSCs promotes functional recovery in rat tibialis anterior muscle. J Tissue Eng Regen Med **6,** 117, 2012.
50. Merritt, E.K., Cannon, M.V., Hammers, D.W., Le, L.N., Gokhale, R., Sarathy, A., Song, T.J., Tierney, M.T., Suggs, L.J., Walters, T.J., and Farrar, R.P. Repair of traumatic skeletal muscle injury with bone-marrow-derived mesenchymal stem cells seeded on extracellular matrix. Tissue Eng Part A **16,** 2871, 2010.
51. Rossi, C.A., Flaibani, M., Blaauw, B., Pozzobon, M., Figallo, E., Reggiani, C., Vitiello, L., Elvassore, N., and De Coppi, P. In vivo tissue engineering of functional skeletal muscle by freshly isolated satellite cells embedded in a photopolymerizable hydrogel. FASEB J **25,** 2296–2304, 2011.
52. Wang, L., Cao, L., Shansky, J., Wang, Z., Mooney, D., and Vandenburgh, H. Minimally invasive approach to the repair of injured skeletal muscle with a shape-memory scaffold. Mol Ther **22,** 1441, 2014.
53. Page, R.L., Malcuit, C., Vilner, L., Vojtic, I., Shaw, S., Hedblom, E., Hu, J., Pins, G.D., Rolle, M.W., and Dominko, T. Restoration of skeletal muscle defects with adult human cells delivered on fibrin microthreads. Tissue Eng Part A **17,** 2629–2640, 2011.
54. Beier, J.P., Stern-Straeter, J., Foerster, V.T., Kneser, U., Stark, G.B., and Bach, A.D. Tissue engineering of injectable muscle: three-dimensional myoblast-fibrin injection in the syngeneic rat animal model. Plast Reconstr Surg **118,** 1113, 2006.
55. Irintchev, A., Langer, M., Zweyer, M., Theisen, R., and Wernig, A. Functional improvement of damaged adult mouse muscle by implantation of primary myoblasts. J Physiol **500,** 775, 1997.
56. Corona, B.T., Wu, X., Ward, C.L., McDaniel, J.S., Rathbone, C.R., and Walters, T.J. The promotion of a functional fibrosis in skeletal muscle with volumetric muscle loss injury following the transplantation of muscle-ECM. Biomaterials **34,** 3324, 2013.
57. Aurora, A., Roe, J.L., Corona, B.T., and Walters, T.J. An acellular biologic scaffold does not regenerate appreciable

de novo muscle tissue in rat models of volumetric muscle loss injury. Biomaterials **67,** 393, 2015.
58. Garg, K., Ward, C.L., Rathbone, C.R., and Corona, B.T. Transplantation of devitalized muscle scaffolds is insufficient for appreciable de novo muscle fiber regeneration after volumetric muscle loss injury. Cell Tissue Res **358,** 857, 2014.
59. Sato, K., Li, Y., Foster, W., Fukushima, K., Badlani, N., Adachi, N., Usas, A., Fu, F.H., and Huard, J. Improvement of muscle healing through enhancement of muscle regeneration and prevention of fibrosis. Muscle Nerve **28,** 365, 2003.
60. Menetrey, J., Kasemkijwattana, C., Day, C.S., Bosch, P., Vogt, M., Fu, F.H., Moreland, M.S., and Huard, J. Growth factors improve muscle healing in vivo. J Bone Joint Surg Br **82, 131**2000.
61. Passipieri, J.A., Baker, H.B., Siriwardane, M., Ellenburg, M.D., Vadhavkar, M., Saul, J.M., Tomblyn, S., Burnett, L., and Christ, G.J. Keratin hydrogel enhances in vivo skeletal muscle function in a rat model of volumetric muscle loss. Submitted 2017. DOI: 10.1089/ten.tea.2016.0458.
62. Deasy, B.M., Lu, A.P., Tebbets, J.C., Feduska, J.M., Schugar, R.C., Pollett, J.B., Sun, B., Urish, K.L., Gharaibeh, B.M., Cao, B.H., Rubin, R.T., and Huard, J. A role for cell sex in stem cell-mediated skeletal muscle regeneration: female cells have higher muscle regeneration efficiency. J Cell Biol **177,** 73, 2007.
63. Deasy, B.M., Schugar, R.C., and Huard, J. Sex differences in muscle-derived stem cells and skeletal muscle. Crit Rev Eukaryot Gene Expr **18,** 173, 2008.
64. Arnold, L., Henry, A., Poron, F., Baba-Amer, Y., van Rooijen, N., Plonquet, A., Gherardi, R.K., and Chazaud, B. Inflammatory monocytes recruited after skeletal muscle injury switch into antiinflammatory macrophages to support myogenesis. J Exp Med **204,** 1057, 2007.
65. Engler, A.J., Sen, S., Sweeney, H.L., and Discher, D.E. Matrix elasticity directs stem cell lineage specification. Cell 126, 677, 2006.
66. Discher, D.E., Mooney, D.J., and Zandstra, P.W. Growth factors, matrices, and forces combine and control stem cells. Science **324,** 1673, 2009.
67. Gilbert, P.M., Havenstrite, K.L., Magnusson, K.E.G., Sacco, A., Leonardi, N.A., Kraft, P., Nguyen, N.K., Thrun, S., Lutolf, M.P., and Blau, H.M. Substrate elasticity regulates skeletal muscle stem cell self-renewal in culture. Science **329,** 1078, 2010.
68. Borselli, C., Storrie, H., Benesch-Lee, F., Shvartsman, D., Cezar, C., Lichtman, J.W., Vandenburgh, H.H., and Mooney, D.J. Functional muscle regeneration with combined delivery of angiogenesis and myogenesis factors. Proc Natl Acad Sci U S A **107,** 3287, 2010.
69. Jones, J.I., and Clemmons, D.R. Insulin-like growth-factors and their binding-proteins—biological actions. Endocr Rev **16,** 3, 1995.
70. Yuksel, E., Weinfeld, A.B., Cleek, R., Waugh, J.M., Jensen, J., Boutros, S., Shenaq, S.M., and Spira, M. De novo adipose tissue generation through long-term, local delivery of insulin and insulin-like growth factor-1 by PLGA/PEG microspheres in an in vivo rat model: a novel concept and capability. Plast Reconstr Surg **105,** 1721, 2000.

Address correspondence to:
George J. Christ, PhD
University of Virginia
415 Lane Road
Building MR5, Room 1231
Charlottesville, VA 22908

E-mail: gjc8w@eservices.virginia.edu

Received: October 19, 2016
Accepted: January 24, 2017
Online Publication Date: April 14, 2017